ACS NANO
Cite This: ACS Nano 2019, 13, 867−877
www.acsnano.org

ARTICLE

Long-Range Activationless Photostimulated Charge Transport in Symmetric Molecular Junctions

Amin Morteza Najarian and Richard L. McCreery*

Department of Chemistry, University of Alberta, Edmonton, Canada T6G 2R3

Supporting Information

ABSTRACT: Molecular electronic junctions consisting of nitroazobenzene oligomers covalently bonded to a conducting carbon surface using an established "all-carbon" device design were illuminated with UV−vis light through a partially transparent top electrode. Monitoring junction conductance with a DC bias imposed permitted observation of photocurrents while varying the incident wavelength, light intensity, molecular layer thickness, and temperature. The photocurrent spectrum tracked the *in situ* absorption spectrum of nitroazobenzene, increased linearly with light intensity, and depended exponentially on applied bias. The electronic characteristics of the photocurrent differed dramatically from those of the same device in the dark, with orders of magnitude higher conductance and very weak attenuation with molecular layer thickness (β = 0.14 nm^{-1} for thickness above 5 nm). The temperature dependence of the photocurrent was opposite that of the dark current, with a 35% *decrease* in conductance between 80 and 450 K, while the dark current *increased* by a factor of 4.5 over the same range. The photocurrent was similar to the dark current for thin molecular layers but greatly exceeded the dark current for low bias and thick molecular layers. We conclude that the light and dark mechanisms are additive, with photoexcited carriers transported without thermal activation for a thickness range of 5−10 nm. The inverse temperature dependence is likely due to scattering or recombination events, both of which increase with temperature and in turn decrease the photocurrent. Photostimulated resonant transport potentially widens the breadth of conceivable molecular electronic devices and may have immediate value for wavelength-specific photodetection.

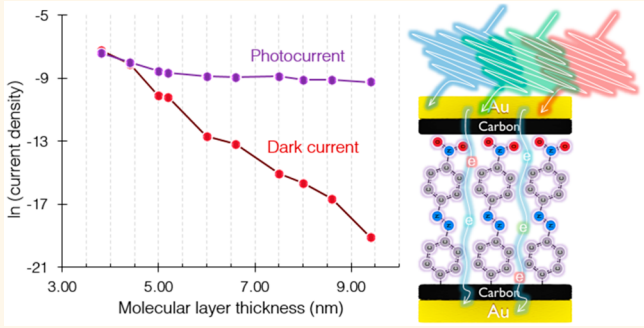

KEYWORDS: *charge transport, molecular electronics, photocurrent, optoelectronics, molecular orbital energy, tunneling barrier, HOMO−LUMO gap, photoinduced transport*

One may consider molecular electronics (ME) as a nanometer-scale version of organic electronics, however, with distinct charge-transport mechanisms over distances of less than 10 nm.[1−4] A core incentive of ME is the desire to benefit from the wealth of organic molecules to design and realize electronic functions not possible with conventional materials.[5−8] In recent years, the emergence of molecular optoelectronics combining optical spectroscopy and quantum-tunneling transport has provided insight regarding the factors controlling transport in ME devices.[9−13] Using light as an external physical stimulus can assist the fundamental understanding of the electron-transport mechanism but also implement photofunctionality into the molecular junction.[5,14,15]

Transport through a few nm of single molecules or a thin molecular layer has been extensively studied, where coherent quantum tunneling is the dominant transport mechanism.[16−18] However, a clear and convincing correlation between transport and molecular energy levels has not been realized in this region of transport, with molecules having distinct orbital energies yielding similar transport behavior.[19−21] This apparent discrepancy can be explained by considering the compression of the tunneling barrier imposed by the energy level realignments or Fermi level pinning at molecule/contact interfaces in completed junctions.[19,22−24] Transition of the charge-transfer mechanism from coherent to alternative incoherent transport is often observed in aromatic molecular junctions with molecule lengths of 4−5 nm.[25−28] The nature and characteristics of the incoherent transport varies for different molecules and strongly depends on the contact coupling strength, delocalization length, and environment of

Received: November 13, 2018
Accepted: December 31, 2018
Published: January 3, 2019

DOI: 10.1021/acsnano.8b08662
ACS Nano 2019, 13, 867−877

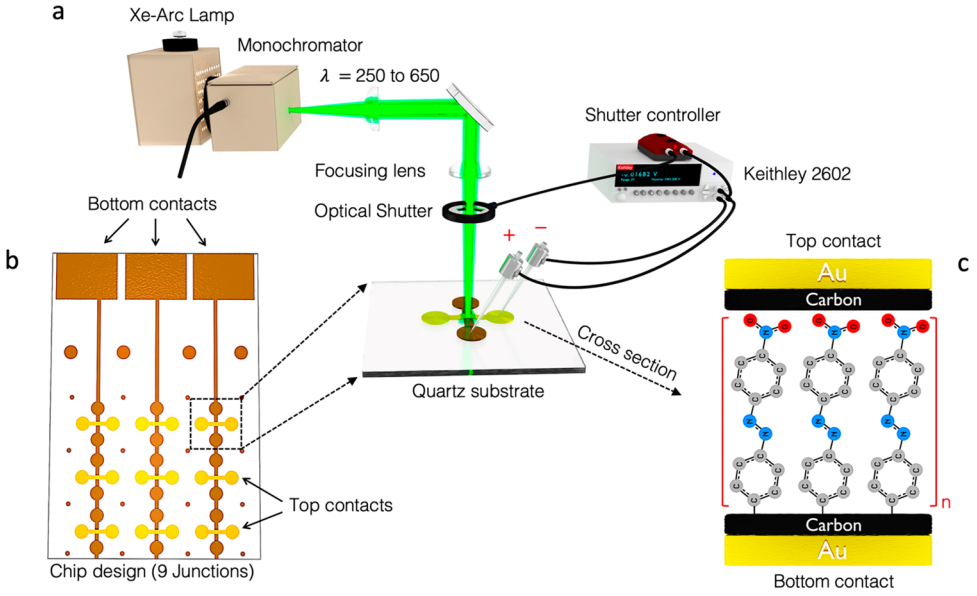

Figure 1. Structure of the molecular junction, chip design, and photocurrent apparatus. (a) Apparatus used for the PC measurement with a continuum source and wavelength selection by a monochromator ($\Delta\lambda$ = 13 nm), modulation by an optical shutter and detection with DC source/measurement unit. (b) Chip design with nine junctions and electrical connections using tungsten probes. (c) Schematic illustration of Quartz/Cr_3/Au_{20}/eC_{10}/NAB/eC_{10}/Au_{20} molecular junction. *n* is the number of repeating units of the oligomer which determine final thickness of the molecular layer ($n \geq 4$). Fabrication details are provided in Supporting Information section 1.

the molecules.[29−31] We showed that for large area carbon/molecule/carbon molecular junctions, transport beyond 5 nm becomes strongly dependent on molecular structure and orbital energies and can be accompanied by light emission or photocurrents.[14,28,32−34] For four different aromatic molecules, analysis of transport in the 4−10 nm thickness range is consistent with sequential tunneling through localized states in the molecular layer.[21] Although one may argue about the details and nature of the transport mechanism, there is an empirical correlation of conductivity with the HOMO−LUMO (H−L) gap of the molecular layer, rather than either H or L offsets from the Fermi level (E_F) of contacts.[21]

Optical spectroscopy has proven to be valuable for characterization of molecular electronic devices, both during fabrication and while in operation. Infrared absorption[35−37] and Raman spectroscopy[38−43] have been implemented to monitor specific local events during charge transfer across the molecular junctions.[44] In addition, application of external illumination in order to generate photocurrent and further stimulate charge transport has attracted experimental and theoretical attention.[34,45−50] Recently, we showed that asymmetry in contact coupling strength is manifested as a built-in potential that drives the photocurrent upon external illumination at zero applied bias.[14] The polarity of the photoinduced potential is dependent on whether the HOMO or LUMO of the incorporated molecules is closer in energy to the electrode Fermi level, which in turn controls the charge redistribution at the interfaces. For thicker molecular junctions (>4 nm) made from eight aromatic molecules with different structures, the photocurrent spectrum corresponds closely to the *in situ* optical absorption spectrum of the junction molecule, indicating that photoexcitation across the optical energy gap is required for observable photocurrents at zero bias.[14] We also showed that larger internal fields and photocurrents are possible using molecular bilayers having total thicknesses less than 10 nm.[51]

Carbon-based large-area molecular junctions permit examination of photocurrents under a wide range of molecular layer thicknesses, applied bias, temperature, and light intensity. We present here the fabrication and experimental platforms that allow us to reliably measure the photocurrent spectrum at elevated external bias. We were able to examine photostimulated charge transport and its dependence on molecular orbitals over a bias range of ±1.5 V, wavelengths of 250−700 nm, and temperatures of 80−450 K. We observed two distinct operating mechanisms (dark and photostimulated) when the molecular layer thickness exceeded the coherent tunneling limit of ∼5 nm. We also determined the relation between contributing experimental factors and stimulated transport. The results presented here should prove useful not only for mechanism diagnosis but also for the incorporation of photofunctionality in molecular electronic devices.

RESULTS

Junction Structure and Photocurrent Measurements.

Symmetric all-carbon molecular junctions were fabricated by established procedures[8,14] on electron-beam deposited carbon (eC) surfaces with the structure and chip design shown in Figure 1. The top contact is approximately 20% transparent, and the nitroazobenzene (NAB) oligomer layer thickness (*d*) was 3.8−9.4 nm, as determined by AFM "scratching".[52] The molecular junction (MJ) area was 0.00125 cm^2, and the illumination area fully covered the entire junction. Many more experimental details including molecular layer grafting procedure are provided in Supporting Information section 1. The apparatus shown in Figure 1 was adapted from that reported previously[14] by the addition of a DC source/measurement unit (Keithley 2602B) and an optical shutter to turn illumination on and off. Most of the results were obtained with the DC apparatus shown, although some used an optical chopper and lock-in amplifier, as noted below.

DOI: 10.1021/acsnano.8b08662
ACS Nano 2019, 13, 867−877

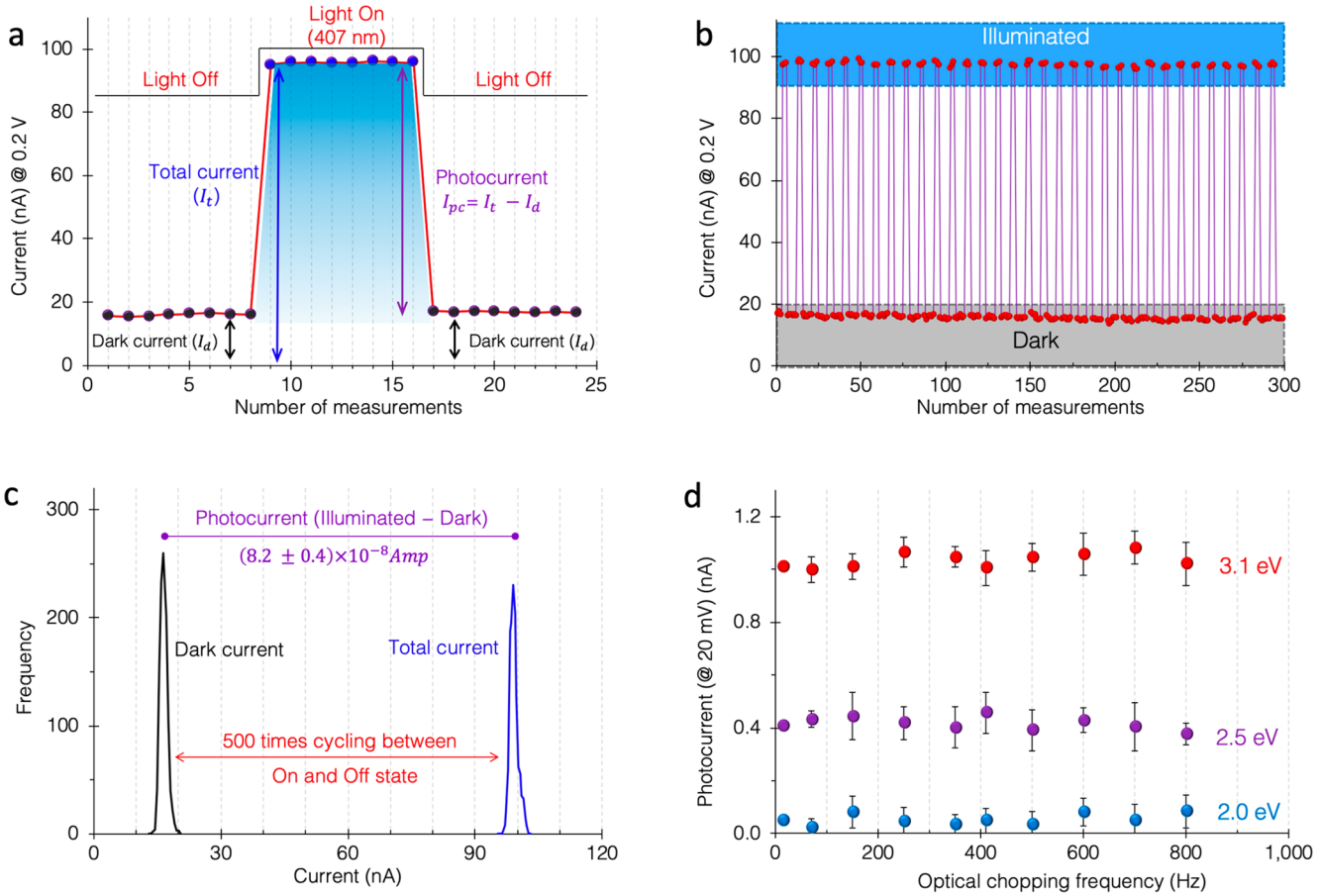

Figure 2. Robustness of the optoelectronic measurement. (a) Observed current for light on/off cycle with constant applied external bias (0.2 V) for 6 nm NAB junction. Power of illumination was 0.8 W/cm^2. (b) The same measurement in panel a repeated for 30 cycles. (c) Histogram of 500 light on/off cycles. (d) Measured photocurrent at V = 20 mV by lock-in amplifier *vs* frequency of the optical chopper from 5 to 800 Hz at three incident light energies. Schematic of the experimental setup is shown in Figure S5.

Detailed procedures and apparatus are provided in the Methods and in the Supporting Information.

A series of DC current measurements for a 0.2 V bias applied to a NAB junction with d = 6.0 nm is shown in Figure 2a, consisting of eight determinations with no illumination followed by eight with the light on. As indicated in Figure 2a, the photocurrent (PC) is defined as the difference between the "light on" and "dark" currents, each of which was averaged over eight measurements. The flowchart of the program used to acquire dark and photocurrents for a range of applied voltages is provided in Supporting Information section 2. Figure 2b shows 30 on/off cycles in succession, with no observable decrease in current magnitudes with repetition. A histogram of 500 on/off cycles is shown in Figure 2c, indicating good stability over a period of at least 1 h. After temporarily replacing the shutter with an optical chopper and using a Xe arc/monochromator source and lock-in amplifier for detection, Figure 2d was obtained for three different incident photon energies. The constant value of photocurrent over a chopper frequency of 5−800 Hz indicates that the PC is tracking the light intensity precisely, at least down to a millisecond time scale. All results subsequent to Figure 2d were obtained as depicted in Figure 2a, with a given point in current−voltage curves being the average of the eight readings with light on or off. The sequence of steps for each data point acquisition is provided in Supporting Information section 2.

Junction Characteristics under Illumination. The Keithley source/measurement unit was programmed to repeat the measurement depicted in Figure 2a for a series of bias values, from which the current/voltage (IV) response for both dark and illuminated conditions could be reconstructed. The results are shown in Figure 3a for NAB (d = 7.5 nm) illuminated at 407 nm (3.69 W/cm^2). The dark current exhibits the sigmoidal shape reported previously[21] and closely resembles the shape and magnitude expected for this thickness obtained with scanning experiments using the same junction structure.[7,21,53] The blue curve in Figure 3a is the same molecular junction when illuminated and has a similar shape but much higher current magnitude. Magnification of the two curves near zero bias shows both a small photocurrent at 0 V and an open-circuit potential (OCP) when the observed current is zero. We reported the zero-bias experiments previously for NAB and other molecules[14] and attributed the photocurrent at zero bias in a structurally symmetric device to a difference in electronic coupling between the molecular layer and the two electrodes. Figure 3b shows the same curves in ln J *vs* bias format (J is the current density in A/cm^2), which demonstrates the photocurrent exceeds the dark current by a factor of >1000 at low bias.

Figure 3c shows the dark responses of MJs with seven different NAB thicknesses ranging from 3.8 to 9.4 nm, all obtained with the same procedure as that in Figure 3a. While the shape of the JV response is similar for all seven, the

DOI: 10.1021/acsnano.8b08662
ACS Nano 2019, 13, 867−877

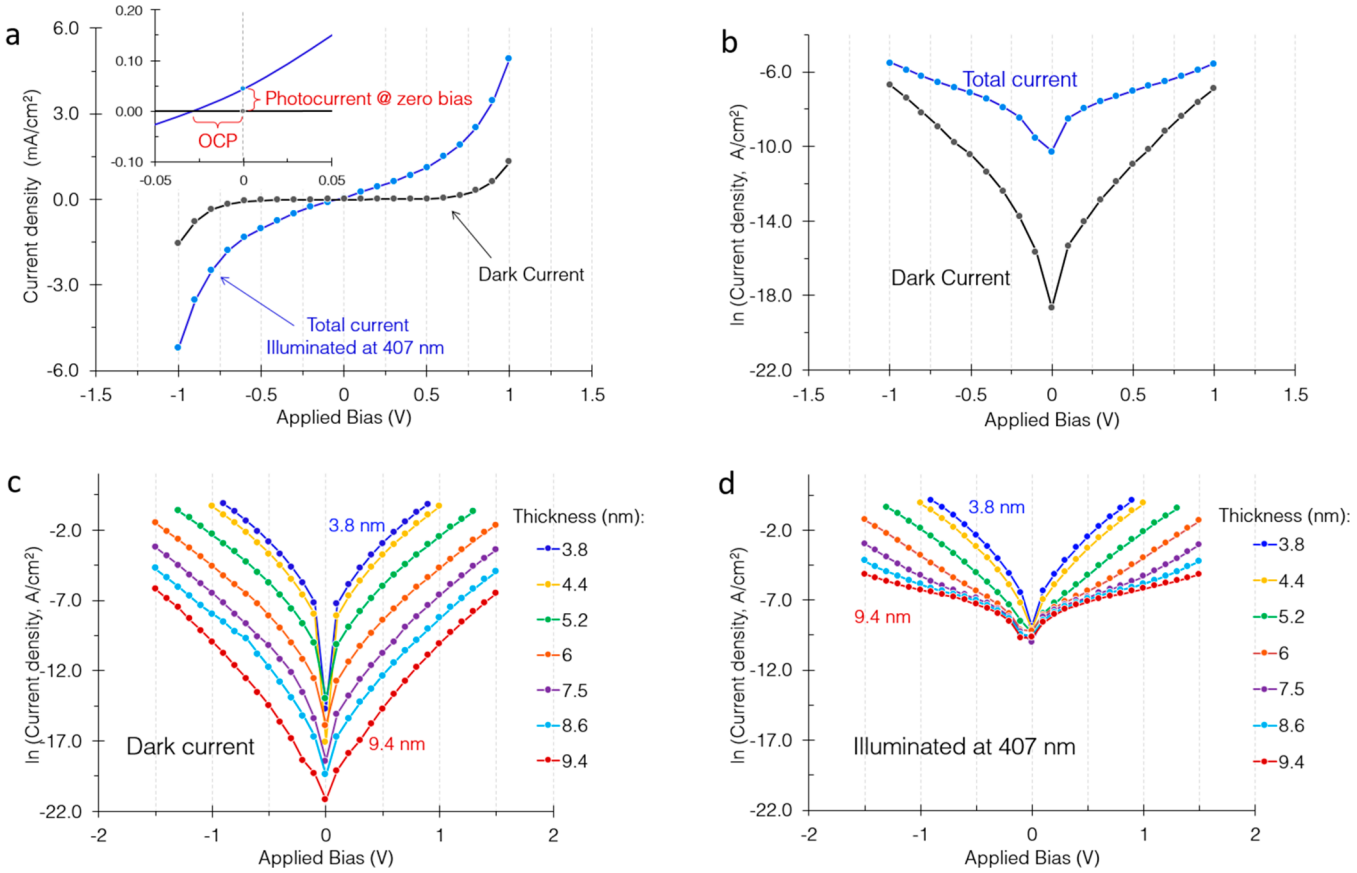

Figure 3. (a) Current density *vs* bias (*JV*) curves for a dark and illuminated junction (dark current is not subtracted) for a 7.5 nm NAB device. Inset is a magnification of the plot origin to illustrate the photocurrent at zero bias and the open circuit potential (OCP). The junction was illuminated by 3.69 W/cm^2 at 407 nm. (b) Semilogarithmic plot of *JV* curves for dark and illuminated junction shown in panel a. (c) Semilogarithmic *JV* curves for NAB junctions without illumination for indicated thickness, each curve is an average of four independent junctions (sample statistics are in Supporting Information section 5). Additional thicknesses are provided in Figure S6. (d) ln *J* *vs* *V* plot for the same samples as those in panel c, following illumination at 407 nm (3.69 W/cm^2).

magnitudes are strongly thickness dependent, as reported previously.[21] When illuminated, the *JV* responses change dramatically, particularly at low bias where the current is nearly independent of thickness once *d* exceeds 5 nm. For example, when $V = 0.1$ V, the dark current decreases by a factor of 7400 for $d = 5.0–9.4$ nm, while the illuminated current decreases by a factor of 2.2 over the same thickness range. This significant difference is discussed in more detail below.

The generality of photocurrent generation under bias was assessed by experiments similar to those of Figure 3a,b but with different molecular layers, *i.e.*, anthraquinone (AQ, $d \sim 7$ nm) and bis-thienyl benzene (BTB, $d \sim 10$ nm). As shown in Figure S9, MJs containing these molecules exhibit much larger current when illuminated, by factors of ~300 for BTB and ~600 for AQ at low bias.

Photocurrent Subtraction and Dependence on Optical Power. The PC determined from the difference between the light and dark responses of Figure 3c,d is plotted *vs* bias in Figure 4a,b in linear and logarithmic formats. Figure 4c is the same data plotted *vs* applied electric field (*E*, MV/cm) instead of bias. The overlap of ln(PC) *vs* *E* for $d > 5$ nm implies that the photocurrent is field-driven, as discussed further below. As shown in Figure 4d, the PC increases with illumination power, and PC is linear with optical power at any tested bias with a correlation coefficient (R^2) higher than 0.98 (example shown in Figure S10). Further analysis of power dependence is provided in Supporting Information section 7 and Figures S11 and S12.

Wavelength Dependence of Photocurrent. Photocurrent spectra were determined over the 240–700 nm wavelength range using the setup shown in Figure 1 with a Xe arc/monochromator source to determine if the applied bias affects the PC spectrum. Figure 5a shows PC spectra for a bias range of +0.3 to −0.3 V, with the dark current subtracted but without correcting for source intensity variation with wavelength. The shape of the spectrum varies little with bias, as shown in Figure 5b, which overlays 10 spectra after normalization to a maximum of 1.0. The small difference between positive and negative bias in the region of 450–550 nm is statistically significant, but of unknown origin. The PC spectrum at $V = 0.3$ V was corrected for source intensity[14,34] and is plotted as PC yield (electrons of current per incident photon) *vs* wavelength in Figure 5c (blue curve). The procedure used for calculation of photocurrent yield (*i.e.*, external quantum efficiency) is provided in Supporting Information section 6. The optical absorbance of the NAB layer inside the molecular junction was determined as described previously[8,14] by subtracting the absorbance of a blank MJ lacking NAB from the absorbance of the complete Au/eC/NAB/eC/Au device. The DFT energy level estimation and absorbance of NAB in different media are provided in Supporting Information section 13. As shown in Figure 5c, the

DOI: 10.1021/acsnano.8b08662
ACS Nano 2019, 13, 867–877

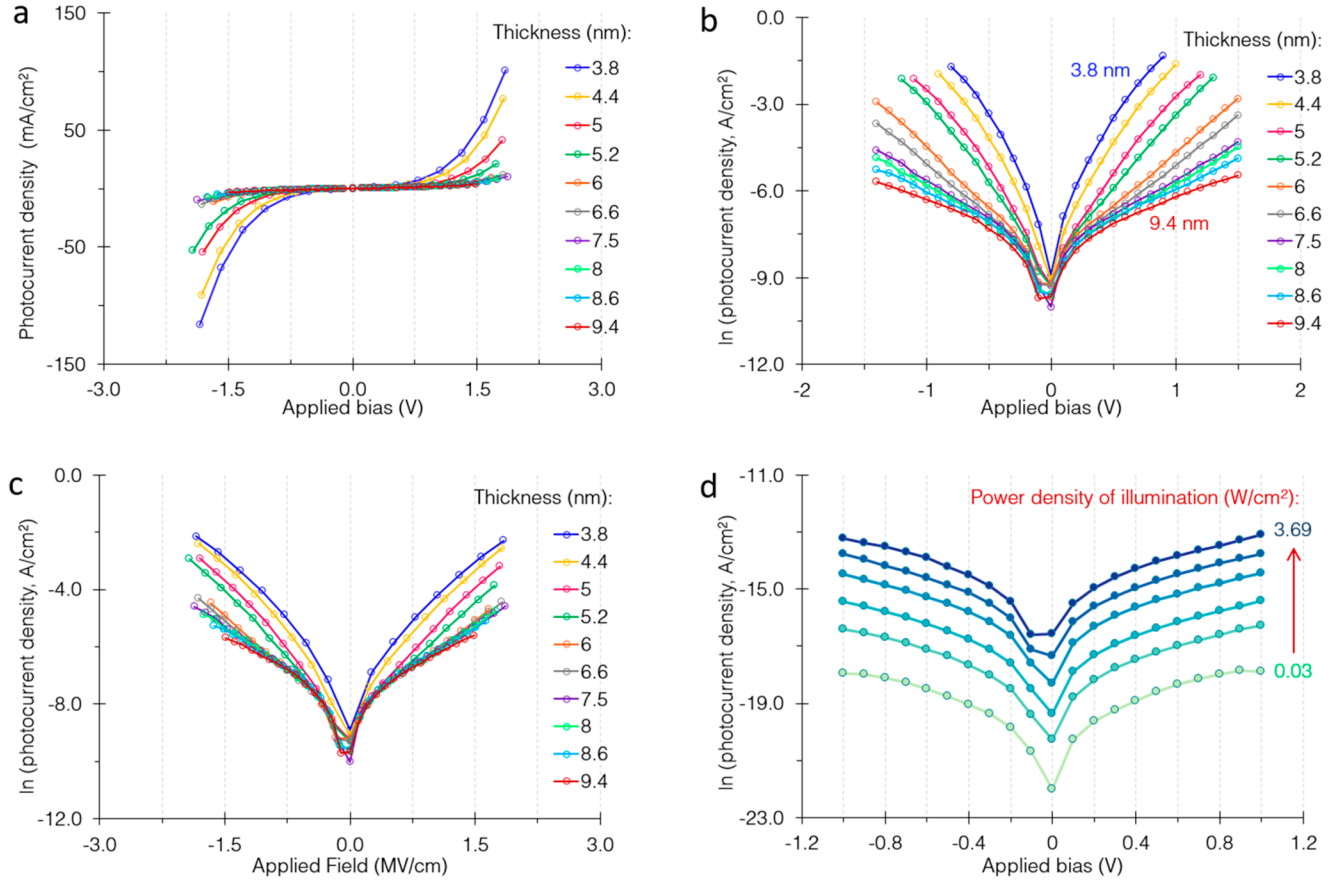

Figure 4. Photocurrent for a range of thicknesses and optical power. (a) PC *vs* voltage for the indicated thicknesses. The power and area of illumination at 407 nm were constant (3.69 W/cm^2) for all junctions. (b) Semilogarithmic plot of curves shown in panel a. (c) ln of photocurrent *vs* applied field (E) rather than bias. (d) ln of *PC vs* applied bias for 9.4 nm NAB junction with illumination intensities from 0.03 to 3.69 W/cm^2 and focused area of ~5 × 10^{-3} cm^2. Area of junctions was 1.25 × 10^{-3} cm^2.

shape of the NAB absorbance spectrum is very similar to that of the PC yield for V = 0.3 V, as was observed previously at zero bias.[14] The linearity of a plot of PC yield *vs* NAB absorbance in Figure 5d confirms this similarity, and 5b indicates that the similarity occurs at all bias values in the range of ±0.3 V. Further analysis of the relation between photocurrent and absorbance is given in Supporting Information section 7.

Relation of Photocurrent to Bias, Thickness, and Temperature. Initial investigations of the bias and temperature dependencies of the photocurrent and dark current are illustrated in Figure 6. As shown in Figure 6a, ln J (dark) is linear with $V^{1/2}$ (R^2 = 0.9993 for V = 0.2 to 1.5 V), which we previously attributed to a bias-induced decrease in tunneling barrier height.[21] The PC also exhibits this relation (R^2 = 0.998 for V = 0.1−1.5 V), albeit with a weaker dependence on $V^{1/2}$. The dark current has the weak temperature dependence shown in Figure 6b, increasing by a factor of ~4.5 between 80 and 400 K, and the increase is similar for all bias values. As shown in Figure S13d, Arrhenius plots of ln J *vs* 1/T are nonlinear with apparent slopes that vary between 6 and 81 meV with temperature (for V = 0.2 V), similar to previous reports.[19,21] In contrast, the PC *decreases* with increasing temperature for all bias values between +0.5 and −0.5 V, as shown in Figure 6c. The opposite trends of dark and PC are apparent in the ln J *vs* T plot of Figure 6d, with the PC decreasing ~35% from 80−450 K, while the dark current increases by a factor of ~4.5 over the same temperature range. For the thinnest MJ with measurable PC over dark current, *i.e.*, d = 5 nm (Figure S14), both the PC and dark responses showed similar trends with temperature as those for d = 7.4 nm, with the dark current increasing by a factor of 4 and the PC nearly constant over the 100−450 K range.

The attenuation plot of ln J(dark) *vs* NAB thickness in Figure 7a has an exponential dependence on thickness characteristic of tunneling, as expected from previous reports,[7,21,54] with an attenuation coefficient (β) of ~1.94 nm^{-1} in the 5−9 nm thickness range. However, the PC for the same devices shows much lower attenuation with distance, with β = 0.14 nm^{-1} in the same thickness range. As shown in Figure 7b, the magnitude of the PC increases with increasing light intensity, but the relative trend remains constant over a 0.12−3.7 W/cm^2 range.

DISCUSSION

Azobenzene and its derivatives are well-known to undergo trans−cis isomerization in monolayers with UV (~350 nm) illumination which can be reversed by ~460 nm light.[55−58] However, the reported time for isomerization is typically 30 min in solution and 45 min in solid state, much longer than the current experimental time scale (<1 min). For example, isomerization of azobenzene in a monolayer bonded to silicon required 5 min of 525 nm illumination @ 0.86 W/cm^2 to yield observable isomerization.[57] The PC responses reported above were independent of chopping frequency, indicating milli-

DOI: 10.1021/acsnano.8b08662
ACS Nano 2019, 13, 867−877

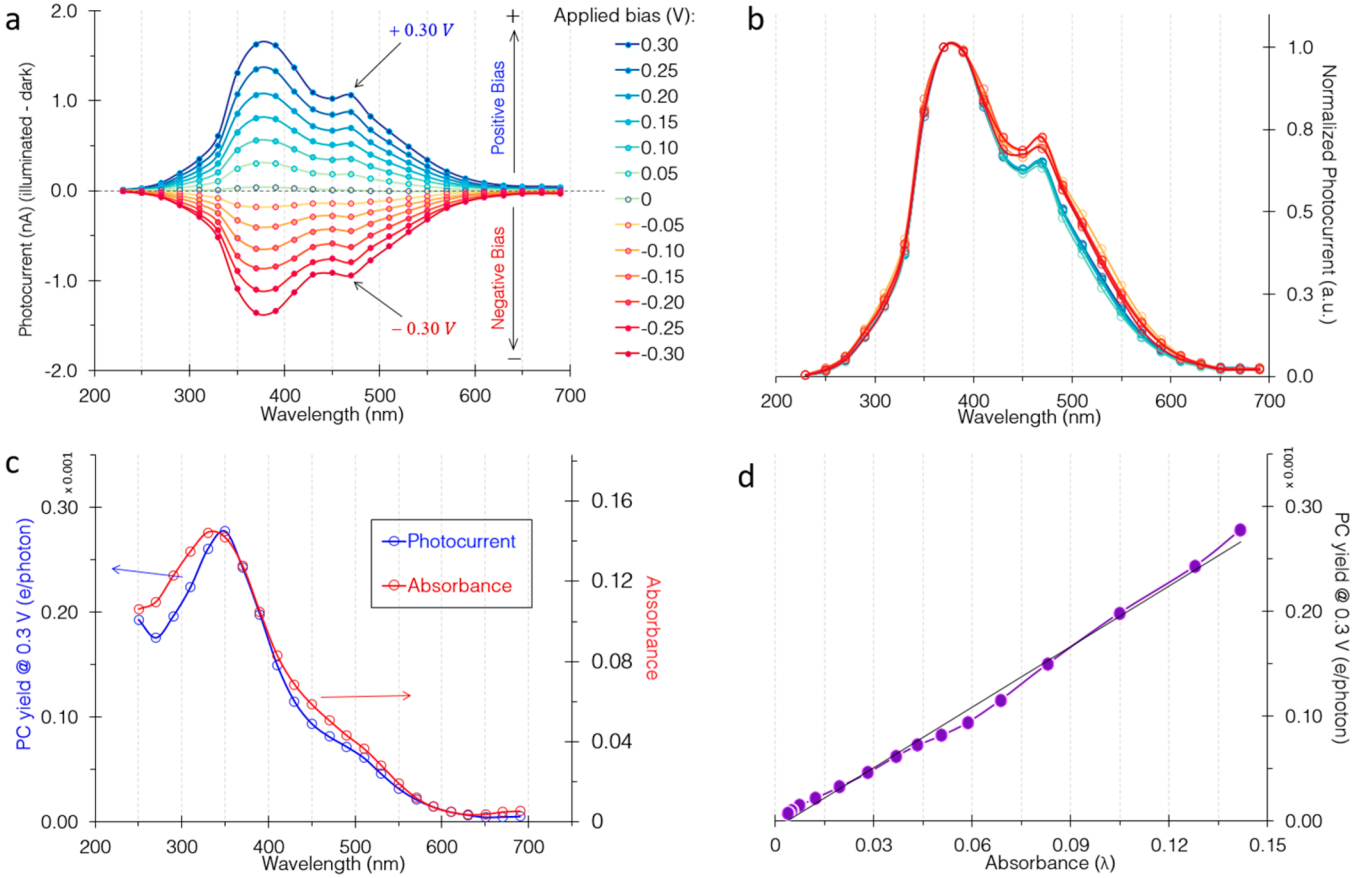

Figure 5. (a) Observed photocurrent spectrum for NAB (d = 8.6 nm) obtained at constant bias, in steps of 0.05 V from −0.3 to +0.3 V. Dark current is subtracted for each bias, but response was not corrected for source intensity variation with wavelength. (b) Overlay of 10 normalized spectra shown in panel (a) with maximum response set to one for each spectrum. (c) PC yield for V = 0.3 V after correction for source intensity compared to the absorption spectrum of the NAB molecular layer within the completed junction. Absorption spectrum was determined for a completed NAB junction (Cr/Au/eC/NAB/eC/Au) followed by subtraction of the spectrum of a blank electrode (Cr/Au/eC/eC/Au).[8,14] PC yield determination is described in Supporting Information section 9. (d) Plot of photocurrent yield *vs* absorbance of NAB molecular layer for the same series of wavelengths shown in panel c.

second or faster response times (Figure 2d), and exhibited no changes or hysteresis with extended exposure to light. Acquisition of the 13 PC spectra in Figure 5a required over 50 min under illumination, and no changes in spectral shape were observed, as shown in the normalized PC spectra of Figure 5b. The similarity of the large increase in current under illumination for BTB and AQ (Figure S9) clearly indicates that the photoeffect is not unique to azobenzene. We conclude that possible isomerization of NAB in carbon-based MJs is too slow to affect the current experiments, if it occurs at all. We previously ruled out an additional possibility for photocurrent generation when d > 4 nm, *i.e.*, internal photoemission (IPE),[34,50] in which carriers are excited in the contacts, then traverse tunneling barriers as "hot electrons".[14] The PCs observed for d > 5 nm for both zero and finite bias track the optical absorption by the molecule and not the contacts (Figure 5). Therefore, IPE could operate for thin devices in the exponential region of Figure 7d (d < 5 nm and β > 1), but it cannot account for the observation of $\beta \sim 0.1$ nm^{-1} in thicker films.

Variation of the applied bias permits direct investigation of the voltage dependence of the photocurrent, and thereby differences between the "dark" and photostimulated transport mechanisms. Figures 3, 4, 6, and 7 show that these differences are both very clear and large in magnitude, with several distinct properties. First, although both dark and PC JV curves show linearity of ln J *vs* $V^{1/2}$, the dark current is more strongly dependent on bias, increasing by a factor of ~10^5 from V = 0.2 to 1.4 V, while the PC increases by a factor of ~15 over the same range (Figures 6a, S21, and S22). As shown in Figure S21, ln J *vs* $V^{1/2}$ linearity is observed in both dark and PC responses for a thickness range of 5.2 to 9.4 nm. Second, the attenuation plots of Figure 7a are similar for dark and PC for d = 3−5 nm but depart significantly for d > 5 nm, where β = 1.94 nm^{-1} for dark current (d = 5.2−9.2 nm) and β = 0.14 nm^{-1} for PC over the same thickness range. The transition of the attenuation slope of the PC is more evident in Figure 7b, which also shows the transition occurs over a range of incident light intensities. Third, the dark current is thermally activated, with an apparent Arrhenius slope increasing from ~6 meV below 250 K to 81 meV above 350 K, while the PC *decreases* with increasing temperature by ~35% for the 80 to 450 K range. This decrease is more evident when ln J is plotted *vs* T in Figure 6d, which compares the ~35% decrease in PC for the 80 to 450 K range to the factor of 4.5 increase for the dark current. Fourth, the PC is linearly dependent on light intensity (Figures 4d, S10, and S11), with the PC at 3.69 W/cm^2 exceeding the dark current by more than 4 orders of magnitude at V = 0.1 V and d = 9.4 nm. All of these differences between dark and PC indicate that PC has a distinct operating

DOI: 10.1021/acsnano.8b08662
ACS Nano 2019, 13, 867−877

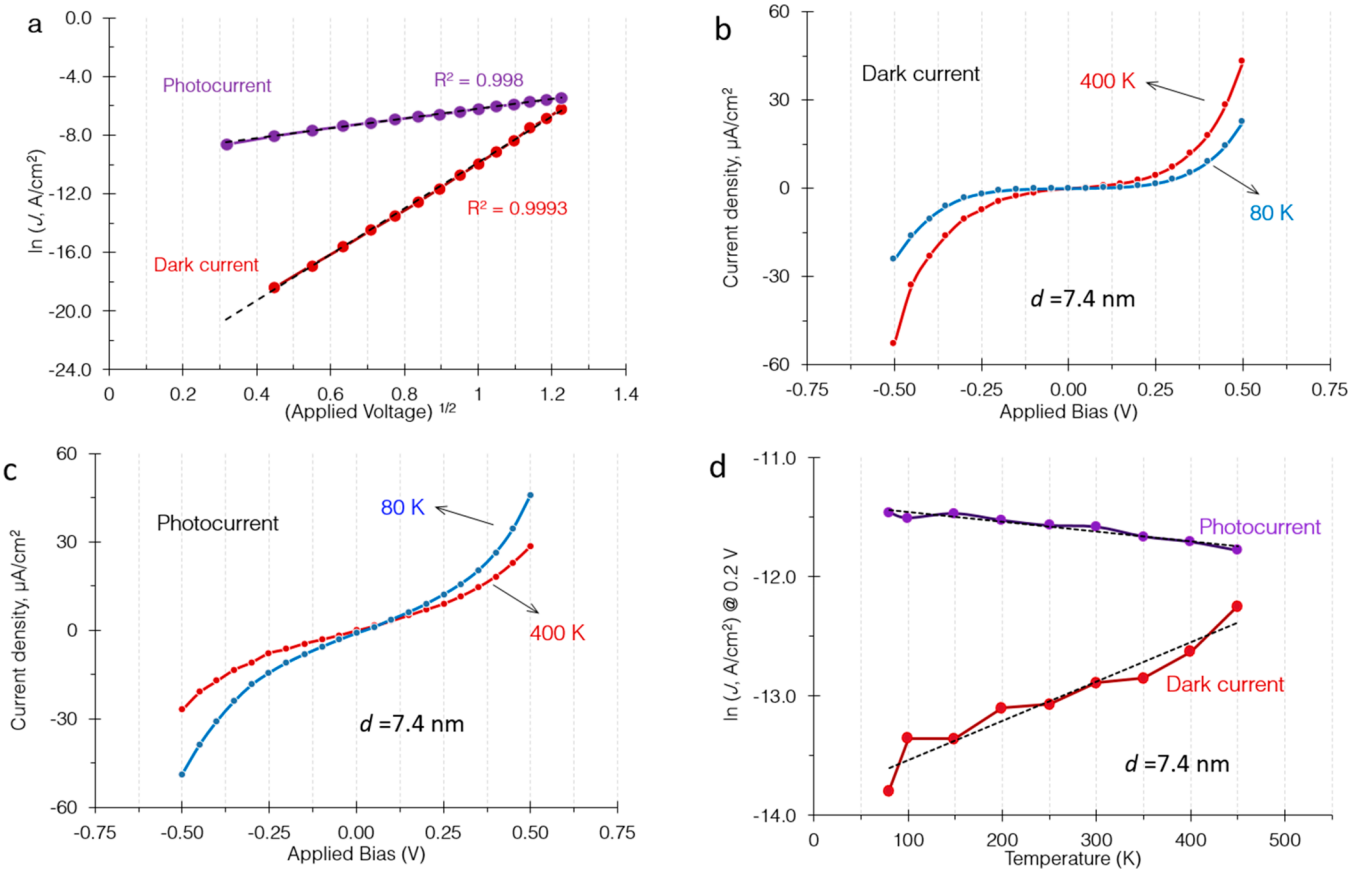

Figure 6. (a) ln J *vs* $V^{1/2}$ plots for photocurrent and dark current for NAB and d = 7.4 nm, MJ area of 0.00122 cm^2. (b) JV curves for NAB in the dark at 80 and 400 K in vacuum. (c) Photocurrent (light−dark) for the same MJ illuminated by 3.69 W/cm^2 diode laser at 407 nm. (d) ln J *vs* T for the same MJ as panels b and c. Arrhenius plots for the same data as panel d are shown in Figure S14d and the apparatus for temperature control is illustrated in Figure S13. Similar results for an additional thickness of 5.2 nm are provided in Figure S15.

mechanism, derived from photoexcited carriers and having different bias, thickness, and temperature dependencies.

To further investigate the transport distance dependence of the PC, Figure 7c shows ln J *vs* d at constant field (0.5 MV/cm), rather than constant bias. The attenuation slope of the component becomes statistically zero for d > 5 nm for all power levels studied. This zero slope implies that the PC transport beyond 5 nm is field controlled and behaves similarly to classical Ohmic conduction and/or transport governed by standard mobility equations such as that in semiconductors, which also predict zero β at constant field. Figure 7c also demonstrates that although illumination power controls the magnitude of the photocurrent, the values and the change in β at $d \sim 5$ nm are not affected by illumination power.

The similarity of the PC yield (e/photon) and the absorption spectrum of NAB within the molecular junction is an important indicator of the probable PC transport mechanism. The zero-bias photocurrent spectra for eight molecules considered previously[14] also are very similar to their optical absorption spectra, and Figures 5c and Figures S17 and S18 indicate that the correlation is maintained under bias as well, at least for $V = \pm 0.3$ V. Clearly, the photocurrent is initiated by absorption of a photon by NAB accompanied by generation of an electron (in the LUMO) and hole (in the HOMO). The steps following optical absorption are the subjects of a large literature on photocurrents in both inorganic[59] and organic[60,61] semiconductors and in heterojunction solar cells,[62] most of which have transport distances exceeding 100 nm. Photoconductance in thick organic semiconductors is activated and involves various hopping mechanisms, often redox exchange with Arrhenius slopes of >100 meV.[60−62] Decreases in conductance with increasing temperature, such as that shown in Figure 6d are rare in thick organic films or semiconductors[59,63] and has been attributed to scattering and bimolecular recombination rate. For single molecule and monolayer molecular junctions, the temperature dependence of the photoconductance has not been investigated to our knowledge, although several mechanisms have been considered theoretically.[9,10,15,46−48]

The weak dependence on length and the activationless transport reported here for photocurrents in NAB molecular junctions are often associated with resonant transport. Resonance between the HOMO or LUMO orbitals and the electrode Fermi level is unlikely for NAB, but resonance is possible between adjacent molecules following photoexcitation. Resonant transport of both electrons and holes in opposite directions could yield the observed photocurrent, provided the exciton binding energy is overcome. As noted by a reviewer, the similarity of the peak maxima for the absorption and PC spectra apparent in Figure 5c implies that the exciton binding energy is small. Since the 407 nm laser used for Figures 6 and 7 has excess energy over the H−L gap of NAB, this excess may overcome the exciton binding energy. Also, the energy offset between excited electron−hole pairs and contact energy level at interfaces may overcome the exciton binding energy, allowing transport of free excited carriers in the

DOI: 10.1021/acsnano.8b08662
ACS Nano 2019, 13, 867−877

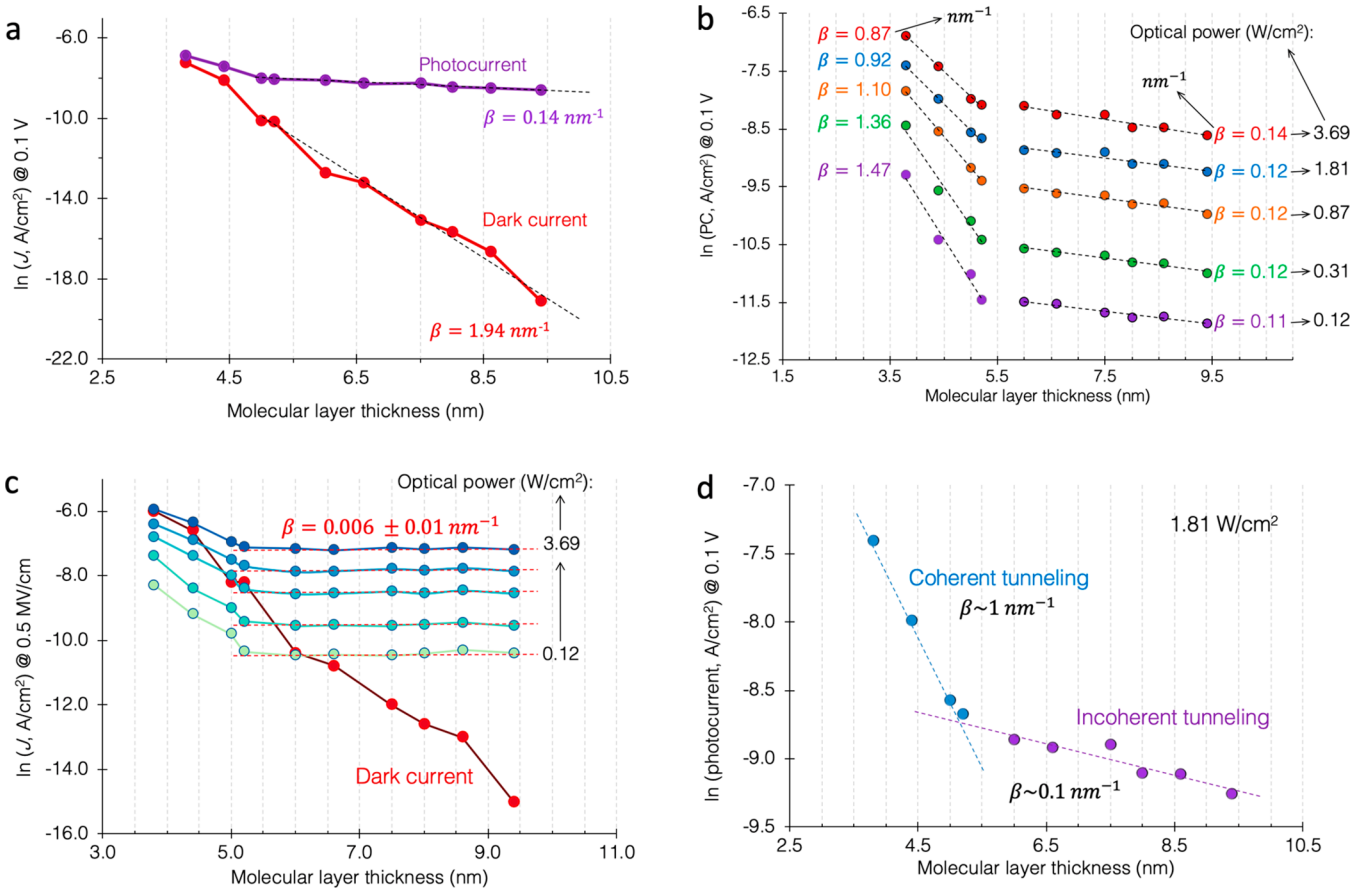

Figure 7. (a) Attenuation plots for the for V = 0.1 V for dark and photocurrent (407 nm, 3.69 W/cm^2). (b) Photocurrents *vs* layer thickness for five illumination powers, with β values indicated. (c) Same data plotted as ln J *vs* d at constant applied field of 0.5 MV/cm (*e.g.*, V = 0.35 V for d = 7 nm). (d) Expanded view of attenuation plot with proposed mechanisms indicated.

direction of the external applied bias. An alternative is a shift in HOMO or LUMO energies by exciton formation, as proposed for single molecules by Dubi et al.[46] If the exciton binding energy is comparable to the H−L gap, the HOMO level could become resonant with the contacts, and exciton formation assists transport. Although resonant transport should not be temperature dependent, the excited electrons are subject to both scattering and recombination, which increase with temperature. The relative rates of transport, scattering and recombination are temperature dependent, with resonant transport becoming more favorable at low temperature. Note that the excited states will have different electronic configurations from the ground state molecules, possibly changing the localization length. In addition, increasing temperature will broaden the distribution of molecular orbital energies as well as the Fermi distribution of carriers in the contacts.

The clear change in attenuation evident in Figure 7 plots at d = 5 nm is strong evidence for a change in mechanism, with both the short-range and long-range mechanisms having very weak temperature dependence. The exponential dependence of ln J with thickness is characteristic of coherent tunneling, and the lower β (~0.87−1.47 nm^{-1}) for the photocurrent in the range of 3−5 nm is consistent with a smaller barrier for tunneling compared to dark current with $\beta \sim 2.5$ nm^{-1}. As indicated in Figure 7d, the transition to lower β for d > 5 nm likely is caused by a change to incoherent tunneling between molecules by one of several "hopping" mechanisms. The linearity of ln J with $V^{1/2}$ shown in Figure 6a for the dark current is consistent with our previous proposal[21] that tunneling barriers are lowered in an electric field, analogous to classical Schottky and Poole−Frenkel behavior, but with weak or absent temperature dependence. The apparent activation energies of 6−81 meV for the dark current are much lower than the reported Schottky barriers for injection into organometallic films,[64] although Schottky injection may still occur with a nonclassical barrier in the case of NAB. The photocurrent shares this relationship, albeit with much weaker voltage dependence and an inverse temperature dependence. Furthermore, the current experiments do not reveal the time scale of transport steps through the NAB film, and reorganization may occur during or after transport. Consistent with many reports, the dark current for d > 5 nm is incoherent and involves several steps and several possible mechanisms depending on the molecules and junction structures. Additional experiments and theoretical analysis are required to determine the "range" of transport in the optically excited molecular junctions, and ultimately, the utility of photon stimulation in molecular electronic devices. Low attenuation of conductivity with thickness for photostimulated charge transfer may permit efficient and activationless transport for significantly thicker molecular layers, with possible utility as wavelength-selective photodetectors.

DOI: 10.1021/acsnano.8b08662
ACS Nano 2019, 13, 867−877

CONCLUSIONS

Illumination of carbon-based nitroazobenzene molecular junctions under external bias with UV−vis light increases junction conductance by 1−4 orders of magnitude for molecular layer thicknesses greater than 5 nm. The photocurrent tracks the *in situ* absorption spectrum of the molecular layer in the wavelength range of 250−690 nm, is linear with light intensity, and is exponentially dependent on the square route of the applied bias. Photocurrents traverse large distances compared to dark current, with an attenuation slope for ln *J vs* thickness of 0.13 nm^{-1} over transport distances of 5−10 nm, compared to the dark value of 1.94 nm^{-1}. The photocurrent magnitude decrease of 35% between 80 and 450 K is opposite that of the activated transport mechanisms in the dark, and is likely due to scattering and recombination which become more likely as *T* increases. We propose that the photo stimulation enables an alternative channel for the transport of excited charges which is additive to the dark current and shows characteristics of efficient resonant transport. It is possible that excited charges delocalize over longer distance and face smaller effective barrier for the transport across the junction in comparison to sequential tunneling of charges in the ground state. The resonant mode of transport should be strongly dependent on molecular structure and orbital energy levels and may be a valuable addition or alternative to molecular electronic devices based on tunneling barriers.

METHODS

Polished fused quartz wafers (Technical Glass Products, Inc.) were diced into chips of 13 mm × 18.5 mm to be used as transparent substrates in the current study to avoid the possibility of stray PC from a silicon substrate. The details of bottom contact deposition, molecular layer grafting and top contact deposition to fabricate Quartz/Cr_3/Au_{20}/eC_{10}/NAB_X /eC_{10}/Au_{20} junction are provided in Supporting Information section 1. We note here that during the eC/Au top contact deposition the chamber backpressure was in the range of 5×10^{-6} to 1×10^{-5} Torr for optimum reproducibility. Optical images of utilized physical shadow masks and a complete chip are shown in Figure S3. Optical absorbance of NAB molecular layer were obtained for complete junction as described previously.[8,14] All current−voltage curves are averages of four independent molecular junctions, and an example of raw data for dark and illuminated currents with their averages and standard deviations is shown in Supporting Information section 5.

A 150 W Xe Arc lamp (Newport model 6256) was used as a broad band light source. Motorized Oriel Cornerstone monochromator model 74004 was used to select and transmit monochromatic light with bandwidth of 13 nm. The output light passed through a Thorlabs ø1 optical beam shutter and was then focused on the junction by a series of lenses. The illuminated molecular junction was contacted via tungsten probes and BNC cables to a Keithley 2602 Source Measurement Unit A (SMU A). The optical shutter was triggered by the voltage output (+2 V) of SMU B to control the state of the shutter (on or off). A custom Visual Basic data acquisition program controlled SMU A and B and collected the output current data point of SMU A. The flowchart of the program is provided in Supporting Information section 2. A Thorlabs 407 nm laser diode powered by a Thorlabs LDC 210C controller, and a TED 200C thermoelectric temperature controller was used as a high power and single wavelength source of illumination. The light intensity was varied between 0.135 and 16.6 mW by a digital controller and measured using a Newport power meter directly above the sample.

Thorlab LDM405 compact laser diode module at 405 nm and 4 mW power was used as a light source to determine the photocurrent temperature dependence. The expriments were done using a Janis ST 500-1 vacuum probe station with temperature controller and liquid nitrogen source. The junction was fixed inside the chamber, and the laser beam was focused on the sample through the mirrors and the glass window of the chamber. The state of the light (on or off) was controlled manually. Further details on the vacuum temperature measurements are shown in Supporting Information section 8.

ASSOCIATED CONTENT

Supporting Information

The Supporting Information is available free of charge on the ACS Publications website at DOI: 10.1021/acsnano.8b08662.

Fabrication conditions; program used to collect photocurrent data; schematic for light chopping frequency-dependent experiment; ln *J vs V* curves for complete set of tested thicknesses; statistics for Cr3/Au20/eC10/NAB8/eC10/Au20; Effect of light on *JV* curves for anthraquinone (AQ) and bis-thienyl benzene (BTB); relation of photocurrent to optical power; temperature dependence of dark and photocurrents; calculation of photocurrent yield (EQE); relation of photocurrent and absorbance of molecular layer; photocurrent yield spectra for NAB at six bias values; BTB photocurrent spectrum under bias; structure, energy levels, and optical absorbance of NAB; plots of ln *J vs* $V^{1/2}$ for various NAB thicknesses (PDF)

AUTHOR INFORMATION

Corresponding Author

*Tel: 780-641-1760. E-mail: richard.mccreery@ualberta.ca.

ORCID

Amin Morteza Najarian: 0000-0002-0455-0451

Richard L. McCreery: 0000-0002-1320-4331

Notes

The authors declare no competing financial interest.

ACKNOWLEDGMENTS

This work was supported by the University of Alberta, the National Research Council of Canada, the Natural Sciences and Engineering Research Council, and Alberta Innovates. The authors thank Drs. Juan Carlos Cuevas, Michael Galperin, and Colin van Dyck for valuable scientific discussions, Dr. Jean-Christophe Lacroix for supplying the BTB precursor, and Bryan Szeto for assistance with LabView programming.

REFERENCES

(1) Vilan, A.; Aswal, D.; Cahen, D. Large-Area, Ensemble Molecular Electronics: Motivation and Challenges. *Chem. Rev.* **2017**, *117*, 4248−4286.

(2) Akkerman, H. B.; Blom, P. W. M.; de Leeuw, D. M.; de Boer, B. Towards Molecular Electronics with Large-Area Molecular Junctions. *Nature* **2006**, *441*, 69.

(3) Jeong, H.; Kim, D.; Xiang, D.; Lee, T. High-Yield Functional Molecular Electronic Devices. *ACS Nano* **2017**, *11*, 6511−6548.

(4) Xiang, D.; Wang, X.; Jia, C.; Lee, T.; Guo, X. Molecular-Scale Electronics: From Concept to Function. *Chem. Rev.* **2016**, *116*, 4318−4440.

(5) Aradhya, S. V.; Venkataraman, L. Single-Molecule Junctions Beyond Electronic Transport. *Nat. Nanotechnol.* **2013**, *8*, 399−410.

(6) Chen, X.; Roemer, M.; Yuan, L.; Du, W.; Thompson, D.; del Barco, E.; Nijhuis, C. A. Molecular Diodes with Rectification Ratios Exceeding 105 Driven by Electrostatic Interactions. *Nat. Nanotechnol.* **2017**, *12*, 797−803.

(7) McCreery, R.; Yan, H.; Bergren, A. J. A Critical Perspective on Molecular Electronic Junctions: There Is Plenty of Room in the Middle. *Phys. Chem. Chem. Phys.* **2013**, *15*, 1065−1081.

(8) Morteza Najarian, A.; Szeto, B.; Tefashe, U. M.; McCreery, R. L. Robust All-Carbon Molecular Junctions on Flexible or Semi-Transparent Substrates Using "Process-Friendly" Fabrication. *ACS Nano* **2016**, *10*, 8918−8928.
(9) Galperin, M. Photonics and Spectroscopy in Nanojunctions: A Theoretical Insight. *Chem. Soc. Rev.* **2017**, *46*, 4000−4019.
(10) Galperin, M.; Nitzan, A. Molecular Optoelectronics: The Interaction of Molecular Conduction Junctions with Light. *Phys. Chem. Chem. Phys.* **2012**, *14*, 9421−9438.
(11) Ivashenko, O.; Bergren, A. J.; McCreery, R. L. Light Emission as a Probe of Energy Losses in Molecular Junctions. *J. Am. Chem. Soc.* **2016**, *138*, 722−725.
(12) Du, W.; Wang, T.; Chu, H.-S.; Wu, L.; Liu, R.; Sun, S.; Phua, W. K.; Wang, L.; Tomczak, N.; Nijhuis, C. A. On-Chip Molecular Electronic Plasmon Sources Based on Self-Assembled Monolayer Tunnel Junctions. *Nat. Photonics* **2016**, *10*, 274−280.
(13) Fainberg, B. D.; Jouravlev, M.; Nitzan, A. Light-Induced Current in Molecular Tunneling Junctions Excited with Intense Shaped Pulses. *Phys. Rev. B: Condens. Matter Mater. Phys.* **2007**, *76*, 245329.
(14) Morteza Najarian, A.; Bayat, A.; McCreery, R. L. Orbital Control of Photocurrents in Large Area All-Carbon Molecular Junctions. *J. Am. Chem. Soc.* **2018**, *140*, 1900−1909.
(15) Gao, Y.; Galperin, M. Simulation of Optical Response Functions in Molecular Junctions. *J. Chem. Phys.* **2016**, *144*, 244106−244106.
(16) Xie, Z.; Bâldea, I.; Oram, S.; Smith, C. E.; Frisbie, C. D. Effect of Heteroatom Substitution on Transport in Alkanedithiol-Based Molecular Tunnel Junctions: Evidence for Universal Behavior. *ACS Nano* **2017**, *11*, 569−578.
(17) Su, T. A.; Neupane, M.; Steigerwald, M. L.; Venkataraman, L.; Nuckolls, C. Chemical Principles of Single-Molecule Electronics. *Nature Reviews Materials* **2016**, *1*, 16002.
(18) Zhang, Y.; Qiu, X.; Gordiichuk, P.; Soni, S.; Krijger, T. L.; Herrmann, A.; Chiechi, R. C. Mechanically and Electrically Robust Self-Assembled Monolayers for Large-Area Tunneling Junctions. *J. Phys. Chem. C* **2017**, *121*, 14920−14928.
(19) Sayed, S. Y.; Fereiro, J. A.; Yan, H.; McCreery, R. L.; Bergren, A. J. Charge Transport in Molecular Electronic Junctions: Compression of the Molecular Tunnel Barrier in the Strong Coupling Regime. *Proc. Natl. Acad. Sci. U. S. A.* **2012**, *109*, 11498−11503.
(20) Tefashe, U. M.; Nguyen, Q. V.; Lafolet, F.; Lacroix, J.-C.; McCreery, R. L. Robust Bipolar Light Emission and Charge Transport in Symmetric Molecular Junctions. *J. Am. Chem. Soc.* **2017**, *139*, 7436−7439.
(21) Morteza Najarian, A.; McCreery, R. L. Structure Controlled Long-Range Sequential Tunneling in Carbon-Based Molecular Junctions. *ACS Nano* **2017**, *11*, 3542−3552.
(22) Van Dyck, C.; Ratner, M. A. Molecular Junctions: Control of the Energy Gap Achieved by a Pinning Effect. *J. Phys. Chem. C* **2017**, *121*, 3013−3024.
(23) Van Dyck, C.; Geskin, V.; Kronemeijer, A. J.; de Leeuw, D. M.; Cornil, J. Impact of Derivatization on Electron Transmission through Dithienylethene-Based Photoswitches in Molecular Junctions. *Phys. Chem. Chem. Phys.* **2013**, *15*, 4392−4404.
(24) Zhirnov, V.; Cavin, R. Chemistry of Molecules or Physics of Contacts? *Nat. Mater.* **2006**, *5*, 11−12.
(25) Amdursky, N.; Marchak, D.; Sepunaru, L.; Pecht, I.; Sheves, M.; Cahen, D. Electronic Transport *Via* Proteins. *Adv. Mater.* **2014**, *26*, 7142−7161.
(26) Choi, S. H.; Risko, C.; Delgado, M. C. R.; Kim, B.; Bredas, J.-L.; Frisbie, C. D. Transition from Tunneling to Hopping Transport in Long, Conjugated Oligo-Imine Wires Connected to Metals. *J. Am. Chem. Soc.* **2010**, *132*, 4358−4368.
(27) Ho Choi, S.; Kim, B.; Frisbie, C. D. Electrical Resistance of Long Conjugated Molecular Wires. *Science* **2008**, *320*, 1482−1486.
(28) Yan, H.; Bergren, A. J.; McCreery, R.; Della Rocca, M. L.; Martin, P.; Lafarge, P.; Lacroix, J. C. Activationless Charge Transport across 4.5 to 22 Nm in Molecular Electronic Junctions. *Proc. Natl. Acad. Sci. U. S. A.* **2013**, *110*, 5326−5330.
(29) Taherinia, D.; Smith, C. E.; Ghosh, S.; Odoh, S. O.; Balhorn, L.; Gagliardi, L.; Cramer, C. J.; Frisbie, C. D. Charge Transport in 4 Nm Molecular Wires with Interrupted Conjugation: Combined Experimental and Computational Evidence for Thermally Assisted Polaron Tunneling. *ACS Nano* **2016**, *10*, 4372−4383.
(30) Selzer, Y.; Cai, L.; Cabassi, M.; Yao, Y.; Tour, J.; Mayer, T.; Allara, D. Effect of Local Environment on Molecular Conduction: Isolated Molecule Vs. Self-Assembled Monolayer. *Nano Lett.* **2005**, *5*, 61−65.
(31) Kuang, G.; Chen, S.-Z.; Wang, W.; Lin, T.; Chen, K.; Shang, X.; Liu, P. N.; Lin, N. Resonant Charge Transport in Conjugated Molecular Wires Beyond 10 Nm Range. *J. Am. Chem. Soc.* **2016**, *138*, 11140−11143.
(32) Ivashenko, O.; Bergren, A. J.; McCreery, R. L. Monitoring of Energy Conservation and Losses in Molecular Junctions through Characterization of Light Emission. *Adv. Elec. Mater.* **2016**, *2*, 1600351.
(33) Bayat, A.; Lacroix, J.-C.; McCreery, R. L. Control of Electronic Symmetry and Rectification through Energy Level Variations in Bilayer Molecular Junctions. *J. Am. Chem. Soc.* **2016**, *138*, 12287−12296.
(34) Fereiro, J. A.; Kondratenko, M.; Bergren, A. J.; McCreery, R. L. Internal Photoemission in Molecular Junctions: Parameters for Interfacial Barrier Determinations. *J. Am. Chem. Soc.* **2015**, *137*, 1296−1304.
(35) Scott, A.; Hacker, C. A.; Janes, D. B. *In Situ* Structural Characterization of Metal/Molecule/Silicon Junctions Using Backside Infrared Spectroscopy. *J. Phys. Chem. C* **2008**, *112*, 14021−14026.
(36) Jun, Y.; Zhu, X. Ftir Spectroscopy of Buried Interfaces in Molecular Junctions. *J. Am. Chem. Soc.* **2004**, *126*, 13224−13225.
(37) Coll, M.; Miller, L. H.; Richter, L. J.; Hines, D. R.; Jurchescu, O. D.; Gergel-Hackett, N.; Richter, C. A.; Hacker, C. A. Formation of Silicon-Based Molecular Electronic Structures Using Flip-Chip Lamination. *J. Am. Chem. Soc.* **2009**, *131*, 12451−12457.
(38) Jiang, N.; Foley, E. T.; Klingsporn, J. M.; Sonntag, M. D.; Valley, N. A.; Dieringer, J. A.; Seideman, T.; Schatz, G. C.; Hersam, M. C.; Van Duyne, R. P. Observation of Multiple Vibrational Modes in Ultrahigh Vacuum Tip-Enhanced Raman Spectroscopy Combined with Molecular-Resolution Scanning Tunneling Microscopy. *Nano Lett.* **2012**, *12*, 5061−5067.
(39) Liu, Z.; Ding, S.-Y.; Chen, Z.-B.; Wang, X.; Tian, J.-H.; Anema, J. R.; Zhou, X.-S.; Wu, D.-Y.; Mao, B.-W.; Xu, X.; Ren, B.; Tian, Z.-Q. Revealing the Molecular Structure of Single-Molecule Junctions in Different Conductance States by Fishing-Mode Tip-Enhanced Raman Spectroscopy. *Nat. Commun.* **2011**, *2*, 305.
(40) Supur, M.; Smith, S. R.; McCreery, R. L. Characterization of Growth Patterns of Nanoscale Organic Films on Carbon Electrodes by Surface Enhanced Raman Spectroscopy. *Anal. Chem.* **2017**, *89*, 6463−6471.
(41) Bergren, A. J.; McCreery, R. L. Analytical Chemistry in Molecular Electronics. *Annu. Rev. Anal. Chem.* **2011**, *4*, 173−195.
(42) Mahmoud, A. M.; Bergren, A. J.; McCreery, R. L. Derivatization of Optically Transparent Materials with Diazonium Reagents for Spectroscopy of Buried Interfaces. *Anal. Chem.* **2009**, *81*, 6972−6980.
(43) Nowak, A. M.; McCreery, R. L. *In Situ* Raman Spectroscopy of Bias-Induced Structural Changes in Nitroazobenzene Molecular Electronic Junctions. *J. Am. Chem. Soc.* **2004**, *126*, 16621−16631.
(44) Martini, I. B.; Barthel, E. R.; Schwartz, B. J. Optical Control of Electrons During Electron Transfer. *Science* **2001**, *293*, 462−465.
(45) Pourhossein, P.; Vijayaraghavan, R. K.; Meskers, S. C. J.; Chiechi, R. C. Optical Modulation of Nano-Gap Tunnelling Junctions Comprising Self-Assembled Monolayers of Hemicyanine Dyes. *Nat. Commun.* **2016**, *7*, 11749.
(46) Zhou, J.; Wang, K.; Xu, B.; Dubi, Y. Photoconductance from Exciton Binding in Molecular Junctions. *J. Am. Chem. Soc.* **2018**, *140*, 70−73.

DOI: 10.1021/acsnano.8b08662
ACS Nano 2019, 13, 867−877

(47) Viljas, J. K.; Pauly, F.; Cuevas, J. C. Modeling Elastic and Photoassisted Transport in Organic Molecular Wires: Length Dependence and Current-Voltage Characteristics. *Phys. Rev. B: Condens. Matter Mater. Phys.* **2008**, *77*, 155119.
(48) Viljas, J. K.; Pauly, F.; Cuevas, J. C. Photoconductance of Organic Single-Molecule Contacts. *Phys. Rev. B: Condens. Matter Mater. Phys.* **2007**, *76*, 033403.
(49) Jia, C.; Migliore, A.; Xin, N.; Huang, S.; Wang, J.; Yang, Q.; Wang, S.; Chen, H.; Wang, D.; Feng, B.; Liu, Z.; Zhang, G.; Qu, D.-H.; Tian, H.; Ratner, M. A.; Xu, H. Q.; Nitzan, A.; Guo, X. Covalently Bonded Single-Molecule Junctions with Stable and Reversible Photoswitched Conductivity. *Science* **2016**, *352*, 1443−1445.
(50) Fereiro, J. A.; McCreery, R. L.; Bergren, A. J. Direct Optical Determination of Interfacial Transport Barriers in Molecular Tunnel Junctions. *J. Am. Chem. Soc.* **2013**, *135*, 9584−9587.
(51) Smith, S. R.; McCreery, R. L. Photocurrent, Photovoltage and Rectification in Large-Area Bilayer Molecular Electronic Junctions. *Adv. Elec. Mater.* **2018**, *4*, 1800093.
(52) Anariba, F.; DuVall, S. H.; McCreery, R. L. Mono- and Multilayer Formation by Diazonium Reduction on Carbon Surfaces Monitored with Atomic Force Microscopy "Scratching". *Anal. Chem.* **2003**, *75*, 3837−3844.
(53) Bergren, A. J.; McCreery, R. L.; Stoyanov, S. R.; Gusarov, S.; Kovalenko, A. Electronic Characteristics and Charge Transport Mechanisms for Large Area Aromatic Molecular Junctions. *J. Phys. Chem. C* **2010**, *114*, 15806−15815.
(54) McCreery, R.; Bergren, A.; Morteza-Najarian, A.; Sayed, S. Y.; Yan, H. Electron Transport in All-Carbon Molecular Electronic Devices. *Faraday Discuss.* **2014**, *172*, 9−25.
(55) Seo, S.; Min, M.; Lee, S. M.; Lee, H. Photo-Switchable Molecular Monolayer Anchored between Highly Transparent and Flexible Graphene Electrodes. *Nat. Commun.* **2013**, *4*, 1920.
(56) Zhang, X.; Wen, Y.; Li, Y.; Li, G.; Du, S.; Guo, H.; Yang, L.; Jiang, L.; Gao, H.; Song, Y. Molecularly Controlled Modulation of Conductance on Azobenzene Monolayer-Modified Silicon Surfaces. *J. Phys. Chem. C* **2008**, *112*, 8288−8293.
(57) Delorme, N.; Bardeau, J. F.; Bulou, A.; Poncin-Epaillard, F. Azobenzene-Containing Monolayer with Photoswitchable Wettability. *Langmuir* **2005**, *21*, 12278−12282.
(58) Velez, M.; Mukhopadhyay, S.; Muzikante, I.; Matisova, G.; Vieira, S. Atomic Force Microscopy Studies of Photoisomerization of an Azobenzene Derivative on Langmuir-Blodgett Monolayers. *Langmuir* **1997**, *13*, 870−872.
(59) Ahn, J.-H.; Ahn, S.-E.; Jeon, Y.; Lee, S.; Song, I.; Kim, J.; Choi, H.; Chung, U.-i. Temperature Dependence of Photocurrent in an Amorphous Gainzno/Inzno Thin Film Transistor. *Appl. Phys. Lett.* **2013**, *103*, 173515.
(60) Platt, A. D.; Kendrick, M. J.; Loth, M.; Anthony, J. E.; Ostroverkhova, O. Temperature Dependence of Exciton and Charge Carrier Dynamics in Organic Thin Films. *Phys. Rev. B: Condens. Matter Mater. Phys.* **2011**, *84*, 235209.
(61) Mizuguchi, J. Temperature Dependence of the Dark Conductivity and Photoconductivity in Evaporated Thin Films of 1,4-Dithioketo-3,6-Diphenyl-Pyrrolo- [3,4-C]-Pyrrole under a High Vacuum or in the Atmosphere of Oxygen or Hydrogen. *J. Appl. Phys.* **1989**, *66*, 3111−3113.
(62) Foertig, A.; Baumann, A.; Rauh, D.; Dyakonov, V.; Deibel, C. Charge Carrier Concentration and Temperature Dependent Recombination in Polymer-Fullerene Solar Cells. *Appl. Phys. Lett.* **2009**, *95*, 052104.
(63) Aleshin, A.; Kiebooms, R.; Menon, R.; Wudl, F.; Heeger, A. J. Metallic Conductivity at Low Temperatures in Poly(3,4-Ethylenedioxythiophene) Doped with ${\Mathrm{Pf}}_{6}$. *Phys. Rev. B: Condens. Matter Mater. Phys.* **1997**, *56*, 3659−3663.
(64) Karipidou, Z.; Branchi, B.; Sarpasan, M.; Knorr, N.; Rodin, V.; Friederich, P.; Neumann, T.; Meded, V.; Rosselli, S.; Nelles, G.; Wenzel, W.; Rampi, M. A.; von Wrochem, F. Ultrarobust Thin-Film Devices from Self-Assembled Metal−Terpyridine Oligomers. *Adv. Mater.* **2016**, *28*, 3473−3480.

DOI: 10.1021/acsnano.8b08662
ACS Nano 2019, 13, 867−877